Preprints of the 2012 20th Mediterranean Conference on Control & Automation (MED), Barcelona, Spain, July 3-6, 2012

Design and development of a hyper-redundant binary active laparoscopic manipulator

Anastasia Mavrommati, Emmanouil Tzorakoleftherakis, and Anthony Tzes, *Senior Member IEEE*

Abstract— **The subject of this article is the development of a prototype hyper-redundant laparoscopic tool. The manipulator consists of cascaded modules which are powered by Shape Memory Alloy wires (NiTi), acting as binary actuators with two stable states. As a result, the repeatability of the manipulator's movement is ensured, alleviating the need for sensing of the manipulator's joint-positions. Each module is composed of three active prismatic actuators in a tripod configuration providing a 3-DOF (two rotational and one translational) maneuverability for each joint. I^2C-networked microcontrollers activate the individual tendons in each joint. Certain design aspects as well as the kinematics of the binary manipulator are presented followed by experimental studies on the laparoscopic tool prototype.**

I. Introduction

The main purpose of Robot-assisted Minimally Invasive Surgery (MIS) is to improve the doctors' performance by providing them with specific tools, capable of replacing a human hand. Several attempts have been made so far, for the construction of such a tool with different actuation mechanisms. In [1] dc-motors are used, resulting in a stiff device, while the medical robot presented in [2], [3] relies on wires to form its shape, without though being able to control each joint separately. Another concept is illustrated in [4], where a snake-like robot using electrostrictive polymer artificial muscle (EPAM) was developed.

In [5]-[9] five medical tools have been developed, exploiting the benefits of actuation methods based on Shape Memory Alloys (SMAs) such as high energy to weight ratio, low voltage activation and low cost. In addition, the absence of frictional parts as well as their small size and weight makes SMAs suitable for small-scale applications.

Overall there is a need to improve the performance of these MIS-laparoscopic tools. A potential improvement would be to advance the ergonomic design by increasing the degrees of freedom (DOFs), resulting in hyper-redundant manipulators. By taking advantage of the additional DOFs complex 3D-curves can be performed, while obstacle avoidance is facilitated.

Further improvements can be attained by utilizing binary actuators, i.e. actuators with two possible states. Binary robots perform discrete movements and thus high repeatability is ensured, while complex feedback sensing is not required. However, as their workspace is non-continuous, a large number of modules is necessary to improve their maneuverability. On the other hand, if the number of modules were to excessively increase, the computational cost for the inverse kinematics problem could be prohibitive. In [14], several previous efforts on hyper-redundant binary manipulators are summarized.

In the sequel, a prototype hyper-redundant laparoscopic tool will be presented (Fig. 1(a)). Due to their previously outlined advantages, SMA wires (NiTi) were selected, acting as binary actuators. The tool consists of kinematically independent modules in a cascade configuration, forming a macroscopically serial robot. It is expandable and, unlike existing designs, it was designed so that the links can be individually controlled. SMA actuation is handled by an embedded electronic circuit, reducing its overall size and increasing its mobility. In addition, a small diameter tube has been placed inside the manipulator cavity, intended for flexible tools or optical fibers.

This paper is structured as follows: Section II describes the design of the surgical tool. In Section III the embedded electronic circuit is analyzed. Section IV provides a kinematic analysis of the manipulator and finally, in Section V, simulation and preliminary experimental results are demonstrated, followed by conclusive remarks.

II. Laparoscopic Manipulator Design

A. Overall Concept

A prototype active laparoscopic surgical tool was studied and developed (Fig. 1(a)). Its diameter and length are 20mm and 250mm respectively, it weighs 80g and consists of 8 modules in total. Since the actuation of the tool is handled by an embedded electronic circuit, no other external mechanism is necessary, allowing its easy transfer and operation.

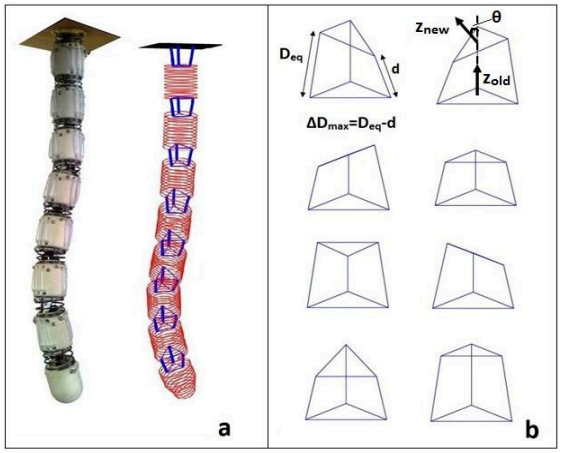

Fig. 1. (a) Laparoscopic manipulator prototype (b) Tripod discrete states

Manuscript received May 13, 2012. The authors are with University of Patras, Electrical & Computer Engineering Department, Rio 26500, Greece. Corresponding author's email: tzes@ece.upatras.gr

978-1-4673-2529-5/12/$31.00 ©2012 IEEE

Three SMA wires, fixed at equilateral triangular locations (tripod configuration), connect each link with the next one and are responsible for the robot motion. The selected SMA configuration, along with the fact that an integrated circuit (IC) has been adjusted to every link, allows for the independent actuation of each SMA and module. The SMAs act as binary actuators with two stable states, i.e. ON and OFF. As a result, each module has 8 discrete states, shown in Fig. 1(b). In order for the desired stroke to be achieved, the SMAs are wrapped around the link's wall. Thus, their final length is much greater than the length of the link. They have been placed inside insulating teflon tubes which diminish the friction caused by the wrapping and provide insulation.

The link is a modified cylinder which carries a slot for the IC and arranged holes for the SMA wrapping (Fig. 2). It was manufactured using rapid prototyping techniques and the selected Duraform HST material provides insulation, strength, and low weight. The consecutive links are connected through a spring which is combined with SMA wires to form a 3-DOF module (Fig. 8b). The module can rotate in a ±8˚ range in 2 degrees of freedom. The 8 concatenated, discretely actuated modules eventually lead to a 24-DOF binary tool. The selection of 8 modules provides a satisfactory workspace of 8^8 possible states (Fig. 3), and at the same time keeps the inverse kinematics problem within our reach. In any case, the number of modules can be increased to meet the requirements of any application.

B. Individual module mechanical design

A counteracting spring was used for the implementation of the module as it was consistent with the particular demands of the SMAs. Specifically:

-It allows the SMAs to be in an elongated condition constantly. Consequently, even a minor displacement of the actuators leads to the spring bending.

-It exercises a return force which restores the actuators to their initial state.

Fig. 4 indicates a simplified model of a bending module. The rotation centre of a tripod is not fixed, but rather changes throughout its motion. However, in the simplified model we estimated the position of the rotation centre *P* for small rotational angles. In addition, we ignored its tripod configuration, assuming a vertical position of its SMA actuators. In the sequel, the overall bending ability of the module is evaluated and the conclusions regarding the arrangement of the SMAs inside the robot are presented.

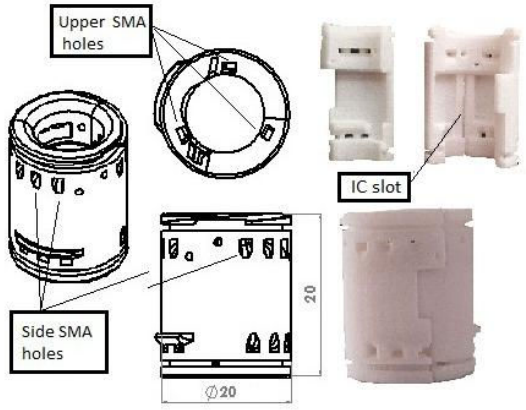

Fig. 2. Single link of the manipulator

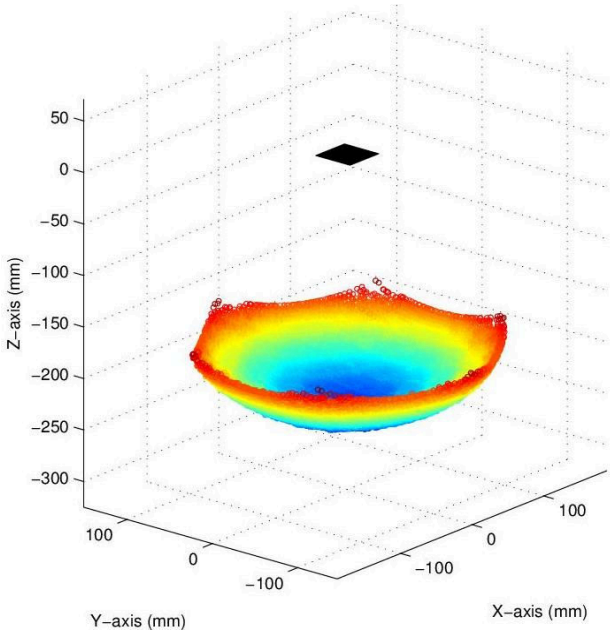

Fig. 3. Workspace of the prototype tool

Of great importance is the distance of the actuators from *P*, namely $R+r$. By increasing this distance, the torque provided by the actuators is increased as well. At the same time however, achieving a specific rotation angle would demand larger actuator displacements and hence longer SMA wires.

Thus, for an 8˚rotation to be obtained, the value of two variables should be considered, namely the SMA displacement dx and the distance $R+r$. Given $R+r$=16 mm, the required displacement is computed as:

$$dx = tan\theta\ (R + r) \xrightarrow{R=10,r=6} dx = 2.24mm \qquad (1)$$

Since the actuators' approximate stroke given by the manufacturer is 3%, the minimum total length of an appropriate SMA is about 75 mm. Following this result, the SMAs were wrapped around the link wall, as indicated in Fig. 7. This arrangement led to both small length links and the desired rotation angle.

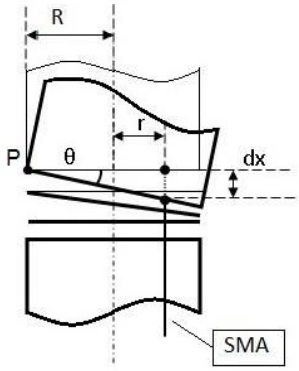

Fig. 4. Simplified model of a bending module

C. Force Considerations

The force required from each actuator was determined at a worst case configuration of the manipulator (Fig. 5) and subsequently, the SMAs with the appropriate diameters were selected.

For this simplified model we approximated the system parameters: the total length k of each link along with the corresponding spring as 30 mm, their total weight w as 0,1 N, and the distance of the SMAs from the centre of rotation as $R+r$=16 mm.

Let τ_{SMA} be the SMA torque and τ_W the weight torque referred to the current axis of rotation. Then:

$$\tau_W = Bx = nw \cdot \frac{nk}{2} = 1{,}5\, n^2 \quad Nmm \qquad \text{n} = 1,2,\dots 8 \qquad (2)$$

where x is the vertical distance of the current rotation centre from the centre of mass of the remaining links, and B their weight. Respectively, let F_{SMA} be the actuator force. Then:

$$\tau_{SMA} = (r+R)F_{SMA} = 16F_{SMA}\, mm \qquad (3)$$

Therefore:

$$\tau_{SMA} > \tau_W \Rightarrow F_{SMA} > 0{,}094n^2 \quad N \qquad \text{n} = 1,2,\dots 8 \qquad (4)$$

For instance, concerning the 3rd link (n=3), the minimum force provided by its actuator should be $3^2 \cdot 0{,}094N = 0{,}85N$. According to the technical specifications, a bended at the middle SMA of 0.20mm diameter would be appropriate. Thanks to that arrangement, two parallel SMA wires are virtually resultant, exerting double force in comparison with the force of a non-bended SMA wire.

III. Embedded Electronics

A. Integrated Circuit

An important part of the manipulator is its electrical design. As stated before, each link is equipped with an embedded IC (Fig. 6(a)), which drives the corresponding SMAs and handles the communication requirements. The ICs were not placed in an external structure, as the total number of wires passing through the base link would greatly affect the diameter and the overall size of the tool. The 12mm×15mm IC consists of a microcontroller (ATTiny44A) and 3 power MOSFETs and it can fit inside the link cavity.

In general, SMAs can be activated simply from the heat generated by a PWM-transmitted current. ATTiny44A can generate up to 3 PWM signals that can be enabled or disabled independently (independent SMA actuation). In our case, the activation of a PWM signal results in the full contraction of the corresponding SMA, i.e. the ON state of the binary actuator.

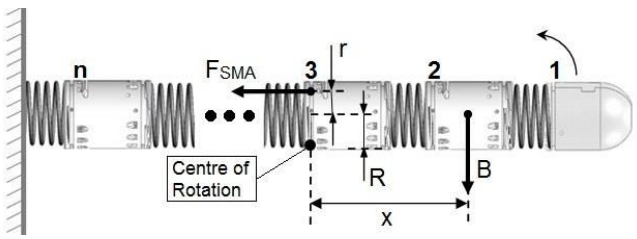

Fig. 5. Extreme configuration forces

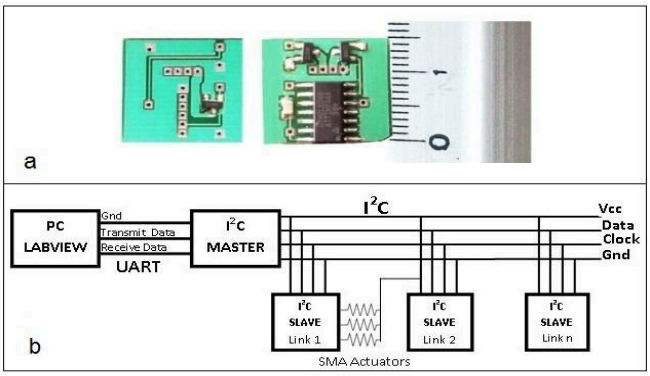

Fig. 6. (a)Top and bottom layer (dimensions in cm) (b) Bus system

B. Communication protocol

Fig. 6(b) depicts the structure of the bus system. The ICs are I^2C-networked, with only four common lead lines required (Vcc, GND, Data and Clock). The I^2C master is implemented by an ATTiny2313A, and the I^2C slaves by the embedded chips described above. The links (slaves) can be addressed individually by the master and receive coded data. The data indicate the activation or not of the PWM signals and hence the desired state of the corresponding SMAs.

The user handles the actuation of the robot using NI LabVIEW to communicate with the I^2C master through RS-232 serial protocol. For addressing a single module and updating the state of the SMAs responsible for its actuation, a set of 8 bits is utilized. This set consists of 5 chip address bits and 3 bits indicating the desired SMA state. For example, the transmitted byte 1101 in binary means that the chip addressed as 1b should activate PWM signals number 1 and 3. This design allows the addressing of 2^5 = 32 different modules.

Fig. 7 displays the details of the individual module's fabrication, including the SMAs and the embedded electronics.

IV. Kinematic Analysis of the Manipulator

A. Forward Kinematics

In order to derive the kinematic model of the manipulator, we take advantage of the joint's tripod-configuration. The model of a 3-DOF tripod with active prismatic actuators is shown in Fig. 8(a).

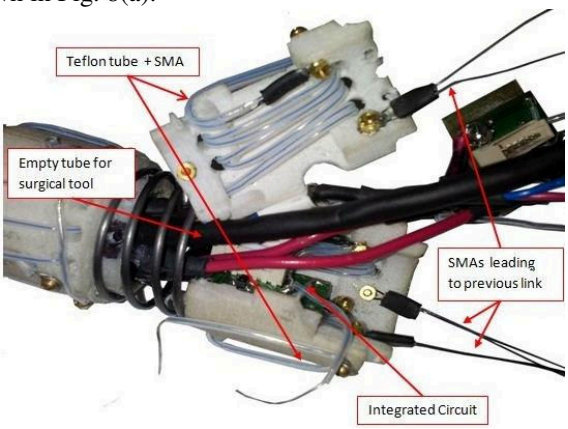

Fig. 7. Individual manipulator joint/link

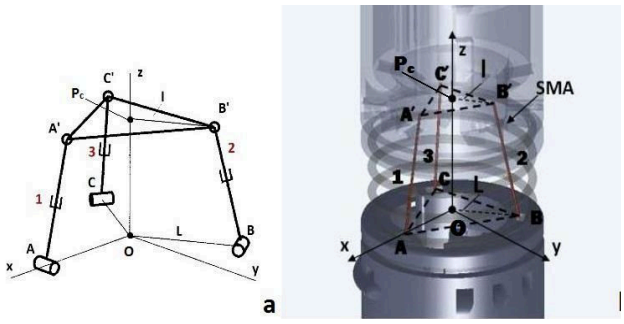

Fig. 8. (a) Spatial 3-DOF Parallel Robot (Tripod Configuration)
(b) Joint Actuation Mechanism

Based on [10], the forward kinematics of the wire-based parallel robot-joint will be presented.

The forward kinematics problem computes the coordinates of the three actuator endings A', B' and C' given as $q_i'=[x_i',y_i',z_i']$, i=1,2,3. The input variables are the lengths of the three prismatic actuators d_i, i=1, 2, 3 measured between the base and the moving platform.

Let u_i, i=1, 2, 3 be the unit vectors along the direction of the points A, B, C. Since the base triangle is equilateral, we have:

$$u_1 = [\sin\left(\frac{\pi}{2}\right), -\cos\left(\frac{\pi}{2}\right), 0]^{\mathrm{T}} \quad (5a)$$

$$u_2 = [\sin\left(-\frac{5\pi}{6}\right), -\cos\left(-\frac{5\pi}{6}\right), 0]^{\mathrm{T}} \quad (5b)$$

$$u_3 = [\sin\left(-\frac{\pi}{6}\right), -\cos\left(-\frac{\pi}{6}\right), 0]^{\mathrm{T}} \quad (5c)$$

Then, the position vectors of the points A, B, C given by $q_i=[x_i,y_i,z_i]^{\mathrm{T}}$, are :

$$q_i = Lu_i \quad (6)$$

where L is the distance from the origin O to A, B and C.

A system of nine equations will be derived, so that the nine unknowns can be computed (x_i',y_i',z_i' for i=1, 2, 3). The first three equations state that the legs of the tripod are forced to rotate on a fixed plane, since the joints on A, B, C were considered to be rotational. Specifically:

$$y_1' = 0 \quad (7a)$$

$$\sqrt{3}x_2' + y_2' = 0 \quad (7b)$$

$$\sqrt{3}x_3' - y_3' = 0 \quad (7c)$$

Imposing the length of each of the SMA wires, d_i, i=1, 2, 3, leads to the three following equations:

$$\|q_i' - Lu_i\| = d_i \quad (8)$$

Finally, the equations showing the constant equal distance between points A′, B′ and C′:

$$\|q_i' - q_j'\| = \sqrt{3}\,l \quad , \qquad i \neq j \quad (9)$$

where l is the distance from the centroid $P_{c\ 3x1}$ of the triangle $A'B'C'$, to its vertices A', B' and C'.

This system of equations (7)-(9) can be solved using numerical methods. Due to the nonlinearity of the equations involved, the number of solutions that could be obtained varies, depending on the initial guess. Given the output variables x_i',y_i',z_i' for i=1, 2, 3, the frame of the moving platform can be determined using the kinematic transformation matrix:

$$T = \begin{bmatrix} X_{new} & Y_{new} & Z_{new} & P_c \\ 0 & 0 & 0 & 1 \end{bmatrix}_{4\times4} = \quad (10)$$

$$= \begin{bmatrix} \frac{q_1' - P_c}{\|q_1' - P_c\|} & \frac{Z_{new} \times X_{new}}{\|Z_{new} \times X_{new}\|} & \frac{X_{new} \times (q_2' - P_c)}{\|X_{new} \times (q_2' - P_c)\|} & P_c \\ 0 & 0 & 0 & 1 \end{bmatrix}_{4\times4}$$

In case of a macroscopically serial manipulator, by repeating the above computation method as many times as the number of the cascaded tripods, we can obtain the exact position of the distal link with respect to the base frame.

Comparing the tripod model (Fig. 8(a)) to the actuation mechanism of the manipulator shown in Fig. 8(b), the spring attached to the consecutive links corresponds to the passive spherical and rotational joints of the tripod whereas the SMA wires act as binary prismatic actuators. The base of the tripod refers to the upper surface of the previous link, while the moving platform is the lower surface of the next link. In our design L=8mm and l=6mm. Taking the above into account, the equations (7)-(9) are solved for each of the 8 discrete states of the tripod depicted in Fig. 1(b). The 8 resulting transformation matrices are fixed and can be used to evaluate the position of the end-effector.

B. Inverse Kinematics

Unlike the forward kinematics case, the inverse kinematics of the laparoscopic tool cannot be reduced to an individual inverse kinematics problem for each tripod. Therefore, our approach is based on the binary nature of the actuators and requires the off-line computation of the tool's discrete workspace (Fig. 3). In order to solve the inverse kinematics problem, we follow the steps outlined below:

Off-line: Find and store the discrete workspace along with the corresponding robot configurations (tripod states), and the 8 transformation matrices given by (10).

1. Input the desired position of the end-effector and define a voxel around it.
2. Search for the points of the workspace that lie inside the voxel. For reduced computation time, the data of the workspace array could be pre-sorted to allow the usage of a binary search algorithm.
3. Find the robot configurations corresponding to the points found at Step 3, using the stored data from Step 1.
4. Choose the robot configuration that maximizes the following criterion: the weighted number of tripods that remain in the same state as in the previous configuration, with a higher weight closer to the base.

This algorithm might not be applicable for applications that demand large number of modules. For this reason, several other inverse kinematics algorithms have been proposed that reduce the computational cost and rely mainly on workspace density functions ([11]-[13]).

In this case however, the contemporary CPU capabilities allow us to follow the proposed "brute force" strategy, as it is more reliable, straightforward and less complicated. The algorithm results in a smooth point-to-point movement of the manipulator which is illustrated in the next section with numerical examples.

C. Tripod Performance Considerations

Following the derivation of the kinematic model, a parametric evaluation of the tripod performance is performed. As a measure of effectiveness, we investigated the variation of the rotation angle θ which was estimated as in Fig. 1(b) and Fig. 4. All the parameters that were examined are described in Table I. Note that this evaluation refers to a typical tripod with prismatic actuators, which unlike the SMAs, can both contract and expand.

Fig. 9 presents the anticipated angle with respect to D_{eq} and the corresponding $\Delta D_{max}/D_{eq}$, which are also depicted in Fig. 1(b). Given a constant $\Delta D_{max}/D_{eq}$ ratio, a greater rotation can be achieved by increasing D_{eq}, which in our case is mainly determined by the spring length. The same will occur if the ratio $\Delta D_{max}/D_{eq}$ increases, when D_{eq} remains constant. In our implementation ΔD_{max} is the contraction of the SMAs.

Likewise, the anticipated angle with respect to the ratios l/L and D_{eq}/L is shown in Fig. 10. It can be seen that for a constant D_{eq}/L ratio, a decrease in the value of l compared to L, leads to a considerable angle rise. In our prototype tool, we have l/L=0.75 and D_{eq}/L=1.5 which results in an angle of 8°, as illustrated.

V. Simulation and Experimental Studies

To evaluate the forward and inverse kinematics of Section IV, we proceeded with a numerical simulation. The ability of our prototype tool to follow a predefined path was tested using the proposed inverse kinematics algorithm. Specifically, the desired path was defined to be a circle inside the workspace of the tool, sampled at 90 points:

$$\begin{pmatrix} 100\sin(t) \\ 100\cos(t) \\ -210 \end{pmatrix}, \qquad t = 0, \frac{2\pi}{90}, \frac{4\pi}{90}, \ldots, 2\pi$$

Fig. 11 illustrates three snapshots of the robot motion. As expected, the state of the modules closer to the base is not significantly altered throughout the simulation, resulting in a smooth overall movement. The bar graph in Fig. 12 is representative of this fact, indicating the variation frequency of each module's state. It can be observed that the base module does not deviate from its initial state, as these additional 3-DOFs are not needed for the specified task.

TABLE I. Tripod Parameters

L	Indicates the size of the tripod base
l	Indicates the size of the moving platform of the tripod
D_{eq}	The length of the tripod legs in the equilibrium state i.e. when no leg is extended or contracted
ΔD_{max}	The maximum displacement of the prismatic actuators (legs)

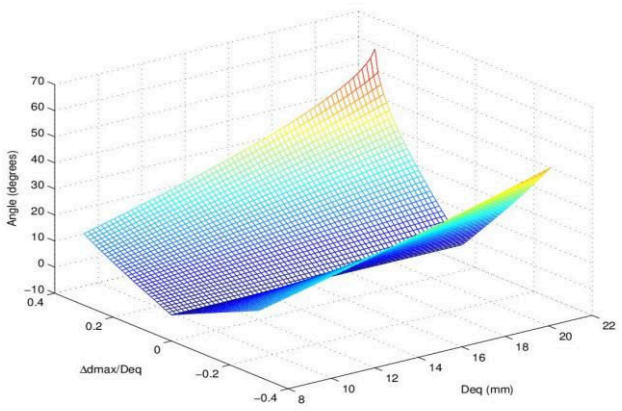

Fig. 9. Parametric angle evaluation

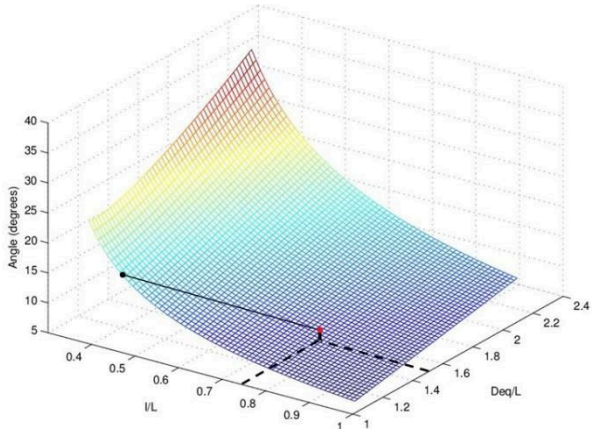

Fig. 10. Parametric angle evaluation

Fig. 12 also shows the actual path followed by the robot in comparison with the desired path, measured for a 4mm edge voxel. The observed error is primarily due to the discretization of the workspace and it may vary depending on the selected voxel size. It must be noted that the online algorithm was completed in a few seconds, since the workspace was computed and stored offline.

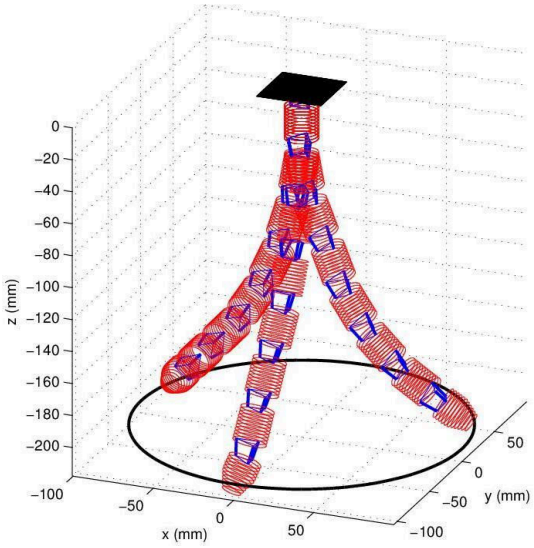

Fig. 11. Demonstration of the robot's movement

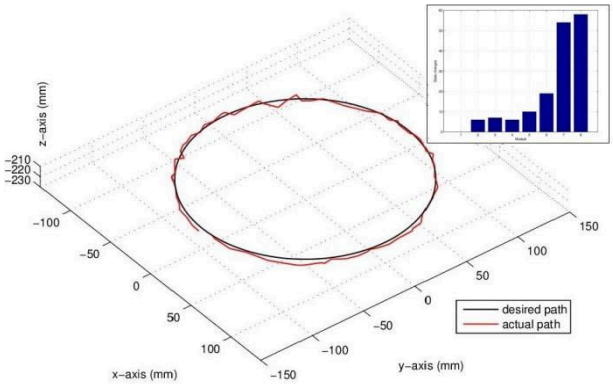

Fig. 12. Simulation results

We have also conducted a primal experiment to test the link addressing and the maneuverability of the manipulator. The following 7 bytes were sent to the master chip, using a USB to Serial cable, each one corresponding to a different module (slave):

Byte1(1100), Byte2(10100), Byte3(11100), Byte4(100010), Byte5(101010), Byte6(110010), Byte7(111010).

A step by step result is demonstrated in Fig. 13. As shown, the expected SMAs were actuated individually, leading to the final desired configuration. The baud rate for the serial communication and the I^2C clock frequency were set at 4800bit/sec and 100 kHz respectively. Taking into account the fact that a complete I^2C write cycle lasts about 25 time periods, each SMA actuator in the active tool can be activated at a time interval of 1.3ms. As a result, the highest actuation frequency of the tool is only limited by the cycling time of the SMAs.

The frequency of the PWM signals was set at 1 kHz, and the duty cycle was determined by the current specifications of the SMAs. Before applying the PWM, the microcontrollers are programmed to provide a high pulse for 1 second in order for the response time of the SMAs to be improved.

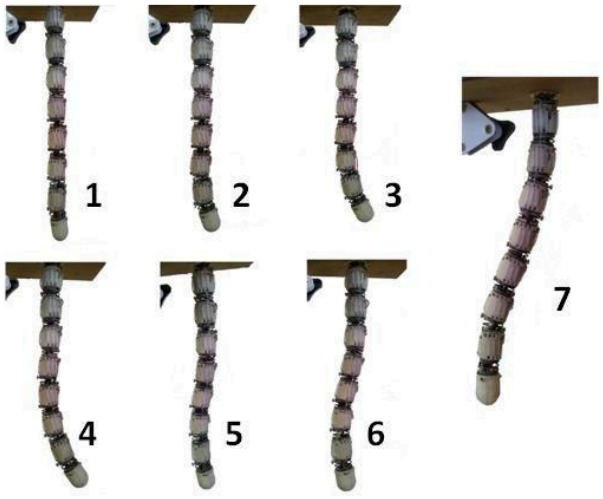

Fig. 13. Sequential step-by-step joint actuation

VI. Conclusions

A prototype MIS-surgical manipulator was developed and a primal experiment has been conducted. The manipulator is modular and expandable and uses SMA wires in a tripod configuration as binary actuators. Thanks to its embedded electronics, the proposed tool is compact and suited for most surgical operations.

Future work will focus on more complex experiments, as well as the minimization of the IC size using a different fabrication method. Subsequently, the overall size of the link will be decreased and the manipulator's maneuverability will improve. For realistic experiments, the tool can be covered with a thin insulating material, ensuring the safety of the patient during the operation.

References

[1] P. Berkelman and J. Ma, "A compact modular teleoperated robotic system for laparoscopic surgery," International Journal of Robotics Research, vol. 28, no. 9, pp. 1198–1215, 2009.

[2] A. Degani, H. Coset, A. Wolf, T. Ota, M. A. Zenati, "Percutaneous intrapericardial interventions using a highly articulated robotic probe". Proceedings, First IEEE/EBIB International Conference on Biomedical Robotics and Biomechatronics (BioRob'06) 2006, pp. 7-12

[3] A. Degani, H. Coset, A. Wolf, M. A. Zenati, "Highly articulated robotic probe for minimally invasive surgery". Conf Proc IEEE Eng Med Biol Soc, pp. 3273 – 3276, 2008

[4] R. Kornbluh, R. Pelrine, J. Eckerle, and J. Joseph, "Electrostrictive polymer artificial muscle actuators," presented at IEEE International Conference on Robotics and Automation, pp. 2147 - 2154 vol.3 Leuven, Belgium, 1998.

[5] V. DeSars, S. Haliyo, and J. Szewczyk, "A practical approach to the design and control of active endoscopes," Mechatronics, Vol.20, No.2, pp. 251-264, 2010.

[6] G. Lim, et al., "Multi-link active catheter snake-like motion," *Robotica*, vol. 14, pp. 499, 1996.

[7] J. Szewczyk, V. de Sars, P. Bidaud, and G. Dumont, "An active tubular polyarticulated micro-system for flexible endoscope," in *Lecture Notes in Control and Information Sciences*, vol. 271 / 2001, *Experimental Robotics VII*: Springer-Verlag, 2003, pp. 179 - 188.

[8] Mingyen Ho, Michael Koltz, J. Marc Simard, Rao Gullapalli, Jaydev P. Desai, "Towards a MR image-guided SMA-actuated neurosurgical robot", In IEEE International Conference on Robotics and Automation - ICRA 2011, pp. 1153 – 1158, Shanghai, China, May 9-13, 2011.

[9] P. Giataganas, N. Evangeliou, Y. Koveos, E. Kelasidi and A. Tzes, "Design and experimental evaluation of an innovative SMA-based tendon-driven redundant endoscopic robotic surgical tool", in 18th Mediterranean Conference on Control and Automation, Corfu, Greece, June 2011.

[10] Clement Gosselin, "A kinematic analysis, optimization and programming of parallel robotic manipulators", Ph.D. Thesis, McGill University, Montréal, 15 June 1988

[11] J. Suthakorn and G. S. Chirikjian, "A new inverse kinematics algorithm for binary manipulators with many actuators", Adv. Robot., vol. 15, no. 2, pp.225 - 244 , 2001.

[12] I. Ebert-Uphoff and G. S. Chirikjian, "Inverse kinematics of discretely actuated hyper-redundant manipulators using workspace densities", in: *Proc. IEEE Int. Conf. on Robotics and Automation*, pp. 139–145, 1996.

[13] Ebert-Uphoff, I. and Chirikjian, G. S., "Efficient workspace generation for binary manipulators with many actuators", J. Rob. Syst. 12(6), 383–400, Jun. 1995.

[14] Suthakorn J., "Binary hyper-redundant robotic manipulator concept", in TENCON 2004. 2004 IEEE Region 10 Conference, Vol.4 pp. 625 – 628, 21-24 Nov. 2004.